

Numerical simulation of crack propagation interacting with microdefects using adaptively refined XFEM

*Z.H. Teng¹, †D.M. Liao¹, S.C. Wu², Z. B. Zhang¹, T. Chen¹, F. Sun¹

¹ State Key Lab. of Material Processing and Die & Mould Technology, Huazhong University of Science & Technology, China

² State Key Lab. of Traction Power, Southwest Jiaotong University, China

*Presenting author: tengzihao@hust.edu.cn

†Corresponding author: liaodunming@hust.edu.cn

Abstract

The presence of the microdefects (microcracks, voids, inclusions) in the vicinity of the macrocrack tip have a significant effect on the crack propagation. Understanding the influence of crack shielding and amplification of microdefects on the SIFs (stress intensity factors) of the macrocrack is critical to accurately simulate crack propagation and predict structural life. The modeling of macrocrack growth involving multiple microdefects is inconvenient due to the different scales and the extension of cracks. In this paper, a multi-level, adaptively refined mesh near the macrocrack tip where the microdefects exist is formulated by the combination of virtual node polygonal element shape function and quadtree meshes. In the framework of XFEM (extended finite element method), the crack growth problem of different scales is unified and solved in one set of meshes. Based on the above approach, we numerically investigated the influence of different kinds of microdefects on the macrocrack propagation. The effectiveness and accuracy of the proposed method are verified by static cracking examples containing microdefects. Then, the influences of parameters such as microdefect position and size on the macrocrack SIFs and the propagating path are studied. The numerical results can provide a basis for component safety assessment.

Keywords: Adaptively mesh refinement, XFEM, Crack propagation, microdefects, virtual node polygonal element

Introduction

Many engineering structures have a large number of microdefects, such as microcracks, voids, inclusions and dislocations. Experimental studies have shown [1-5] that the presence of microdefects has a significant effect on the propagation of macrocrack. Due to the difference in the position and shape of microdefects, it may cause an amplification or shielding effect to the main crack. Accurate analysis of the influence of microdefects on the macrocrack is critical to assessing the service life of the structures. In the last century, analytical methods were used to

study the influence of microdefects on the macrocrack under certain conditions [6-10]. However, analytical methods have some limitations and it is difficult to deal with complex forms of microdefects.

In recent decades, numerical simulation methods have been widely used to deal with the interaction of the macrocrack and microdefects. There are two main methods commonly used, namely the continuum mechanics approaches and the discrete approaches [11, 12]. In the former method, the regions containing microdefects were represented as inclusions with effective mechanical constants. However, this method may lead to a decrease in computational accuracy, and in particular, the local stress concentration caused by microdefects can not be accurately modelled. While in discrete methods, microdefects are explicitly modelled, which can better analyze the interaction of the macrocrack and microdefects. Based on the widely used FEM, a lot of researches have been done on the interaction of the macrocrack and different types of microdefects [13-16]. For crack propagation problems with complex structures involving multiple microdefects, the conventional FEM is not effective since the remeshing process can not be avoided. To overcome the difficulties of remeshing, several methods have been developed, such as the boundary element method [17], meshless method [18], extended finite element method (XFEM) [19]. Among them, the XFEM has gained the most attention due to the feature that the discontinuities can be independent of the mesh.

In our previous work [20], a dynamic multi-level adaptive mesh refinement method and the corresponding VP-XFEM for crack propagation problems were proposed. Compared with the traditional XFEM and meshless methods, this method can obtain better accuracy, convergence, and computational efficiency. Based on the proposed mesh refinement method, the minimum mesh size can reach 1/100 of the original size when the refinement level reaches 7. With this method, multi-level mesh refinement is only performed on the local region where microdefects exist, and the problems at different scales can be unified into a set of mesh without additional processing. Therefore, this paper will extend this algorithm to study the influence of microdefects on macrocrack propagation.

The current research mainly focuses on the effect of microcracks on static macrocrack, little attention is paid to the interaction of growing macrocrack and microdefects [21]. Researches that comprehensively consider the effects of microcracks, voids and inclusions on macrocrack propagation are quite limited. Therefore, the VP-XFEM algorithm is used in this paper to consider the effects of microcracks, microvoids and inclusions on macrocrack propagation.

Numerical formulation

In this section, we briefly describe the composition of VPM shape functions and their continuity at hanging nodes. According to the properties of the VPM shape function, a multi-level adaptive mesh refinement method for microdefects and growing macrocrack is proposed. On this basis, the specific form of VP-XFEM is derived.

VPM shape function and its properties

Polygon elements have gained wide applications in the field of computational methods due to

their strong flexibility. The VPM uses polynomials as the approximation function based on the partition of unity (PU), which permits the direct usage of the Hammer integral and the Gauss integral as employed in standard FEM. This feature makes VPM easy to be applied to XFEM.

Assuming that a polygon domain Ω whose boundary is enclosed by n nodes $\{P_1, P_2, \dots, P_n\}$ in sequence. By introducing the centroid of the polygon P_k (virtual node), the domain can be divided into n non-overlapping virtual sub-triangles $\{T_1, T_2, \dots, T_n\}$. By considering a point P_l with the coordinate (x, y) , which is located in the virtual sub-triangle T_i , the VPM shape function has the following form

$$\Phi_l(\mathbf{x}) = W_{I,i}(\mathbf{x}) \left[(\delta_{il} + \delta_{jl}) \varphi_{VP,i}(\mathbf{x}) + \varphi_{VP,k}(\mathbf{x}) \phi_l(\mathbf{x}) \right] + W_{II,i}(\mathbf{x}) \phi_{VP,i}(\mathbf{x}) \quad (1)$$

where $W_{I,i}$ and $W_{II,i}$ are the weight functions of the constant strain triangular element (CST) and the least-squares method (LSM) in the i -th virtual sub-triangle; $\varphi_{VP}(\mathbf{x})$ and $\phi_{VP}(\mathbf{x})$ are shape functions based on the area coordinates of CST and LSM, respectively. The specific formulations can be found in Ref. [22]. It is worth mentioning that the virtual node P_k is only used for the calculation of the shape function and will not introduce additional degrees of freedom.

VPM shape function continuity test at hanging nodes

Taking the quadrilateral elements as an example (see Fig. 1), one of the initial four large elements is divided into four small elements ①, ⑤, ⑥, and ⑦. Thus the elements ② and ③ have the hanging nodes of d and e . For the VPM, all elements are considered as polygonal elements with n nodes, while n is changeable. In this manner, there are no hanging nodes any more. Fig. 1 (b) shows the segmentation of polygonal elements when using the VPM shape functions. The handling of the elements of ② and ③ is just in the same way as other elements, except that one more virtual sub-triangle is generated. Fig. 1 (b) and (c) show the VPM shape functions at nodes d and e , respectively. It is clearly implied that the VPM shape functions possess a good continuity even near the hanging nodes.

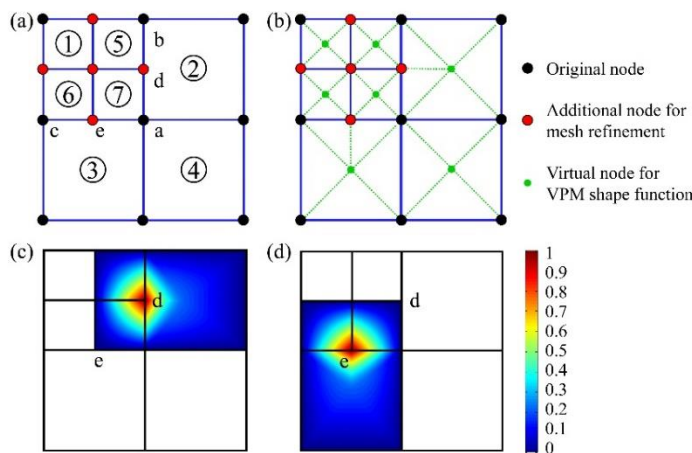


Fig. 1 Mesh refinement of quadrilateral element and the continuity test of VPM shape functions: (a) mesh refinement and the nodes distribution; (b) element division for the calculation of VPM shape functions; (c) the VPM shape function of node d ; (d) the VPM shape function of node e .

Based on the properties of VPM shape functions, an adaptive mesh refinement method for the discontinuities and the corresponding VP-XFEM are proposed by the combination of VPM and XFEM. Since VP-XFEM uses the polynomial shape functions of polygonal elements, it is distinctly different from other methods. The resultant conforming shape functions as well as special integration for sub-elements are not required.

Adaptively mesh refinement

In order to accurately simulate the effects of microdefects on the macrocrack, it is necessary to set fine meshes at the regions containing microdefects or near the crack tip of the macrocrack. Since the size of the microdefects is much smaller than the size of the macrocrack (only 1/100 or even 1/1000), when the quadtree structure is adopted, the refinement levels will reach 8 to 10. Due to the difference in the refinement levels, a lot of hanging nodes are generated in the transition zone between the coarse mesh and the fine mesh. On the other hand, the area to be refined will constantly change because of the crack growth. Therefore, it is also necessary to consider dynamic mesh refinement and coarsening. The previous section shows that VPM is well suited for dealing with non-uniform meshes with hanging nodes. All of the meshes are treated as polygon elements and handled in the same way.

Based on the properties of the VPM shape function, a dynamic adaptive multi-level mesh refinement and coarsening method is proposed in this section. Two sets of meshes are introduced to deal with the refinement process. The initial background mesh with coarse elements (called the base mesh here) is stored by the first meshing set and keeps the same throughout crack growth steps. The second meshing set is created dynamically with growing crack tips. In our previous work [\[20\]](#), the mesh refinement method for the crack propagation problem has been described in detail, but the microvoids and inclusions were not considered. Therefore, the mesh refinement method is further improved for the circular discontinuities (inclusion or hole interface).

Fig. 2 shows a single-step mesh refinement with three circular discontinuities and one main crack. In order to clearly show the refined mesh, only the level 3 refinement is shown in this example, but the process of refining level 8 and above is exactly the same. For crack propagation problem, multiple sub-steps need to be calculated, and each sub-step needs to perform a single-step mesh refinement. Fig. 3 presents the flowchart of the multi-step dynamic mesh refinement around the discontinuities with VP-XFEM. In each sub-step, meshes around the discontinuities are refined based on the initial input mesh. Then in the next sub-step, the crack information is updated, and the mesh refinement is performed again based on the new positions of the crack tips as well as the initial input mesh. At this time, the elements refined in the previous sub-step around the crack tips do not need to be refined due to the moving of the crack tips, so these elements can be maintained as the initial coarse elements. In this way, the dynamic changing of the refined area around the crack tips can be realized, which fulfills the mesh coarsening naturally. Here, a schematic diagram of the refined meshes for the calculation of crack growth containing multiple discontinuities is shown in Fig. 4.

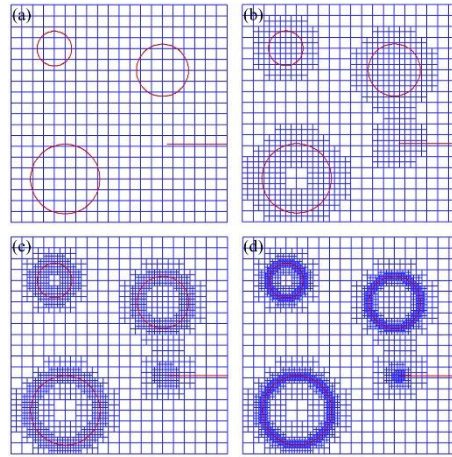


Fig. 2 The mesh refinement around the discontinuities: (a) initial mesh and the location of the discontinuities; (b) one-level refined mesh; (c) two-level refined mesh; (d) three-level refined mesh.

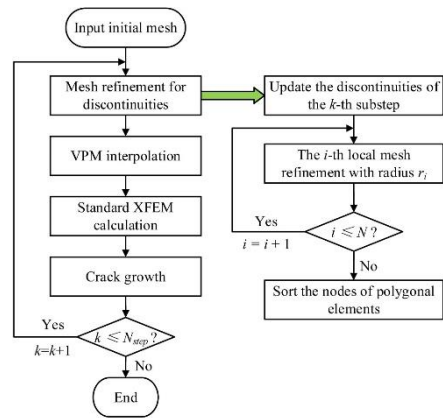


Fig. 3 The flowchart for the multi-step dynamic mesh refinement during a typical crack growth simulation in heterogeneous material.

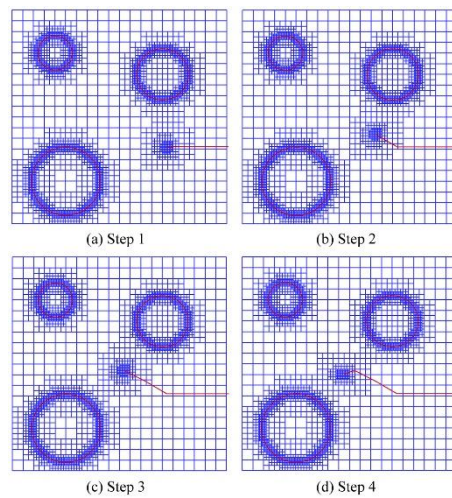


Fig. 4 The refined meshes during a typical crack growth simulation in heterogeneous material with VP-XFEM.

VP-XFEM approximation

By introducing the VPM shape functions into the XFEM displacement approximation with cracks, holes and inclusions [23-26], the VP-XFEM approximation for discontinuities in 2-D can be written as

$$\begin{aligned}
 \mathbf{u}^h(\mathbf{x}) = & \sum_{i=1}^n \Phi_i(\mathbf{x}) \mathbf{u}_i + \sum_{i \in n_r} \Phi_i(\mathbf{x}) [H(\mathbf{x}) - H(\mathbf{x}_i)] \mathbf{a}_i \\
 & + \sum_{i \in n_A} \Phi_i(\mathbf{x}) \sum_{j=1}^4 [\beta_\alpha(\mathbf{x}) - \beta_\alpha(\mathbf{x}_i)] \mathbf{b}_i^j \\
 & + \sum_{i \in n_i} \Phi_i(\mathbf{x}) [\varphi(\mathbf{x}) - \varphi(\mathbf{x}_i)] \mathbf{c}_i \\
 & + \sum_{i \in n_h} \Phi_i(\mathbf{x}) [\psi(\mathbf{x}) - \psi(\mathbf{x}_i)] \mathbf{d}_i
 \end{aligned} \tag{2}$$

The nodes associated with elements completely cut by the crack are enriched by the Heaviside function $H(\mathbf{x})$. $H(\mathbf{x})$ takes the value +1 on one side of the crack and -1 on the other side of the crack. $\beta_\alpha(\mathbf{x})$ is the crack tip enrichment function, which is used to enrich the nodes associated with elements partially cut by the crack. In the polar coordinate system r and θ of the crack tip, $\beta_\alpha(\mathbf{x})$ is defined as below

$$\beta_\alpha(r, \theta) = \left\{ \sqrt{r} \sin \frac{\theta}{2}, \quad \sqrt{r} \cos \frac{\theta}{2}, \quad \sqrt{r} \sin \frac{\theta}{2} \sin \theta, \quad \sqrt{r} \cos \frac{\theta}{2} \sin \theta \right\} \tag{3}$$

The nodes of elements cut by the inclusions and material interfaces are enriched by $\varphi(\mathbf{x})$ which is defined as [25]

$$\varphi(x) = \sum_{i \in n_i} N_i(x) |\phi_i| - \left| \sum_{i \in n_i} N_i(x) \phi_i \right| \tag{4}$$

where ϕ_i is the level set function, $N_i(x)$ is the standard FEM shape function. The nodes of elements cut by the holes are enriched by $\psi(\mathbf{x})$ which takes the value of 1 outside the hole and 0 inside the hole.

Numerical results and discussion

In this section, several numerical examples are given to study the effects of microdefects on the propagation of macrocrack. All the examples are solved by VP-XFEM. The material properties of the plate in all examples is set as $E = 50$ kPa, $\nu = 0.3$. The steady crack propagation of linear elastic material under plane strain condition is considered. In order to ensure the accuracy of the calculated SIFs at the crack tip, the radius of the integration region is four times the size of

the mesh near the crack tip when using the interaction integral.

Influence of a microcrack on the macrocrack propagation

In this section, the influence of the position and shape of microcracks on the macrocrack propagation is studied. The computational model in Fig. 5 is considered. The length of the microcrack is $l=1$ mm, the distance between the macrocrack tip and the center of the microcrack is $s=1.25$ mm. The upper and lower boundaries of the plate were subjected to a load of $\sigma=1$ kPa. Studies have shown that [11], the inclination angle φ of the microcrack and its angle θ with the macrocrack tip have a great influence on the SIFs at the macrocrack tip. With the change of θ and φ , the microcrack can either cause crack shielding or crack amplification. Therefore, the angle $\theta=60^\circ, 90^\circ, 120^\circ$ are considered, and for each case, the inclination angle φ is increased with increment of 30° , $\varphi=0^\circ, 30^\circ, 60^\circ, 90^\circ, 120^\circ, 150^\circ$. For the VP-XFEM, an initial mesh of 19×19 is used. The refinement level is 8 and the refinement radius α_r is 0.15. The growth of microcrack is not considered in this example. The growth increment of the macrocrack is set to $\Delta a_0=0.1$ mm, and the total number of sub-steps is 20.

The variation of SIFs at the macrocrack tip during the crack growth process is shown in Fig. 6. When θ is 60° , φ has a great influence on the value of K_1 at the macrocrack tip. When θ is 90° , φ has some influence on the K_1 in the early stage of crack propagation, but the influence becomes very small in the later stage. When θ is 150° , we can see that the influence of φ on K_1 is really small as the curves are basically overlapping. It can be concluded that only at the front region of the macrocrack tip, the inclination angle φ of the microcrack has a great influence on the SIFs.

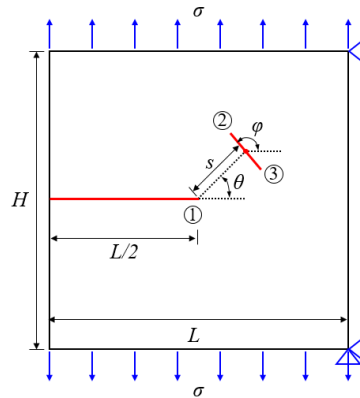


Fig. 5 Sketch of macrocrack growth problem in presence of a microcrack (Unit: mm).

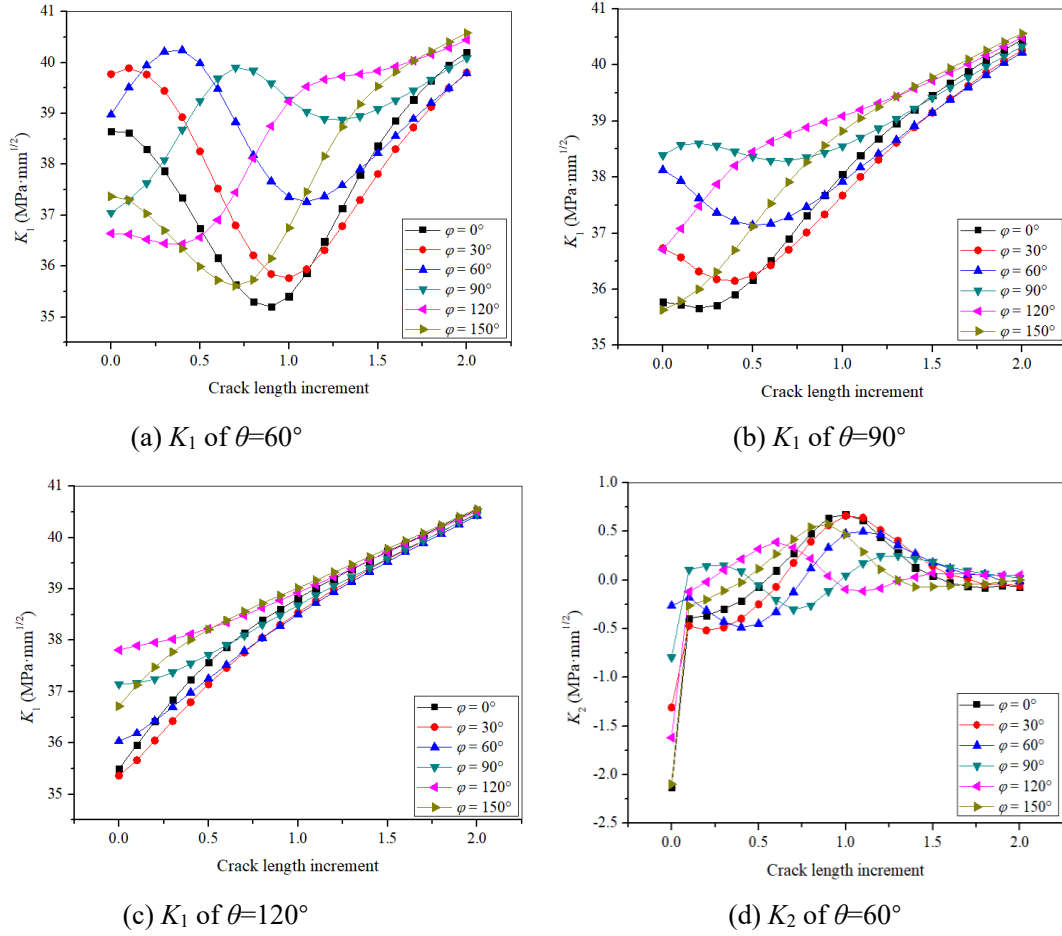


Fig. 6 The variation of SIFs at the macrocrack tip during the crack growth process in presence of a microcrack.

Influence of a microvoid on the macrocrack propagation

In order to investigate the effect of the microvoid on the macrocrack propagation, the numerical example in Fig. 8 is considered. The boundary conditions and material properties are consistent with the first example. The diameter d of the microvoid is kept constant at 2 mm. Different a values (1.86mm, 2.33mm, 3.00mm) are chosen and θ gradually increases from 0° to 90° in increments of 30° . The parameters of the VP-XFEM are set as follows: the initial mesh is 19×19 , the refinement level is 8, and the refinement radius is 0.15. The increment of crack propagation is $\Delta a_0 = 0.15$ mm, and the total number of sub-steps is 20. When the crack intersects the microvoid, the calculation is stopped.

Fig. 8 shows the variation of K_1 at the macrocrack tip during the crack growth process at different values of a . It can be seen that the value of a does not change the tendency of the microvoid to affect the macrocrack during its propagation process. While microvoid have different effects on macrocrack at different values of θ . When the values of θ are 30 and 60 degrees, the microvoid always enhances the K_1 value at the macrocrack tip. But for $\theta=90^\circ$, the microvoid causes a shielding effect. When $\theta=60^\circ$, the microvoid causes a amplification effect in the early stage of crack propagation, after reaching a certain length, the amplification effect

changes to a shielding effect.

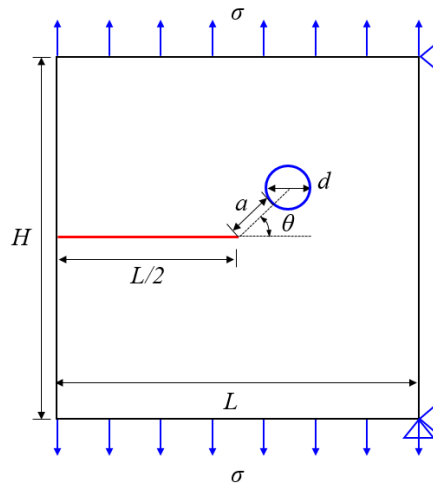


Fig. 7 Sketch of macrocrack growth problem in presence of a microvoid (Unit: mm).

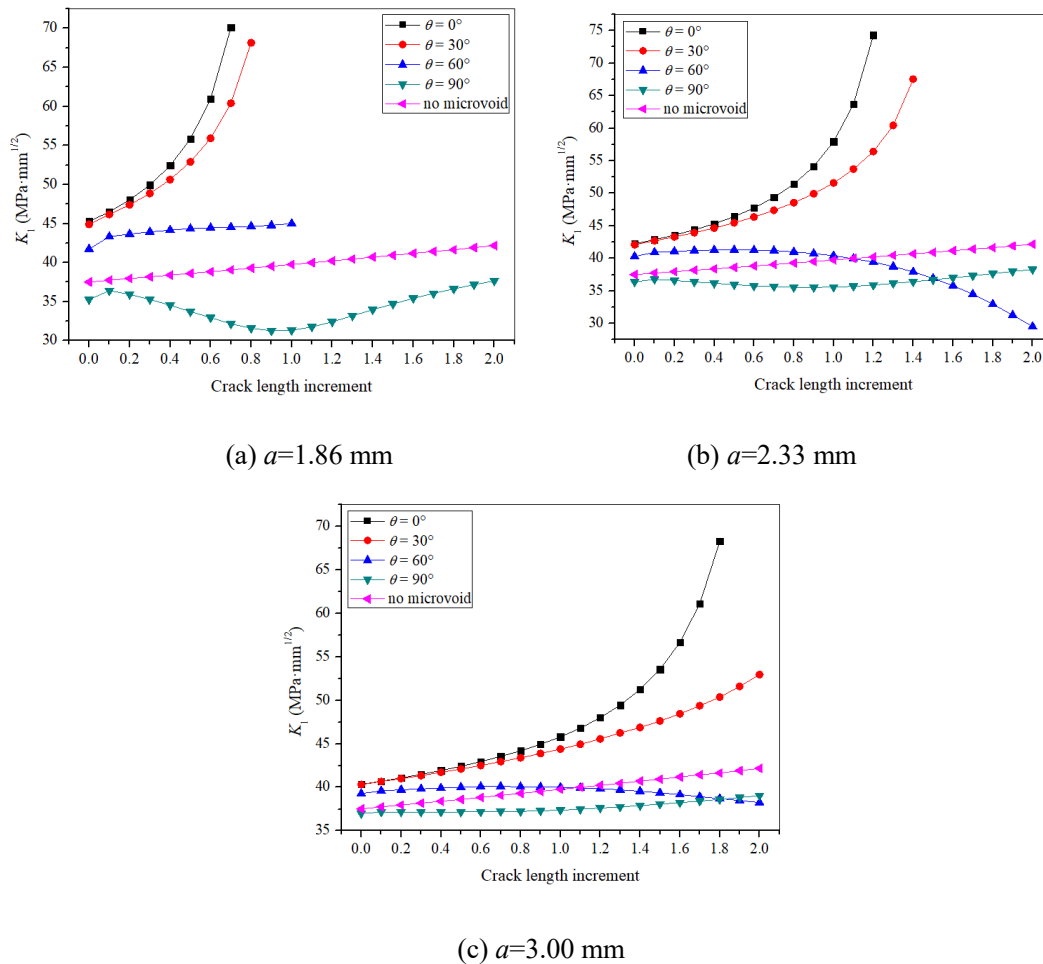


Fig. 8 The variation of K_I at the macrocrack tip during the crack growth process in presence of a microvoid.

Influence of a microinclusion on the macrocrack propagation

In order to study the influence of microinclusion on macrocrack propagation, consider the example shown in Fig. 9. The size and material of the plate, the location of the macrocrack, and the boundary conditions remain the same as in the first numerical example. A circular microinclusion of diameter d is placed near the macrocrack tip. The distance between the center of the microinclusion and the macrocrack tip is s , and the angle of the line connecting the crack tip and the center of microinclusion is θ . In order to investigate the influence of different materials and different inclusion sizes on the macrocrack propagation, the center of the microinclusion is fixed as $s=3.0$ mm, $\theta=30^\circ$. Inclusion in two sizes and two materials are considered, $d_1=2.0$ mm, $d_2=1.6$ mm, and $E_1=25$ kPa, $E_2=100$ kPa. The parameters of the VP-XFEM are set as follows: the initial mesh is 19×19 , the refinement level is 8, and the refinement radius is 0.15. The increment of crack propagation is $\Delta a_0=0.2$ mm, and the total number of sub-steps is 20.

Fig. 10 shows the variation of SIFs at the macrocrack tip during the crack growth process. It can be seen that the larger the inclusion size, the greater the effect on the macrocrack when the elastic modulus of the inclusion is the same. For inclusions of the same size, soft microinclusion causes an amplification effect to the K_1 of macrocrack in the early stage of crack propagation. When the macrocrack expands to a certain length, soft microinclusion causes an shielding effect. While the case of hard microinclusion is just the opposite. For the variation of K_2 , it shows a similar pattern. Soft microinclusion will attract the macrocrack to growth in its direction. While for hard microinclusion, the crack extends away from its direction.

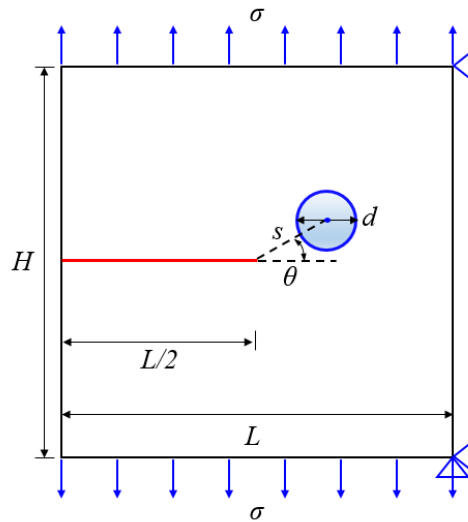


Fig. 9 Sketch of macrocrack growth problem in presence of a microinclusion (Unit: mm).

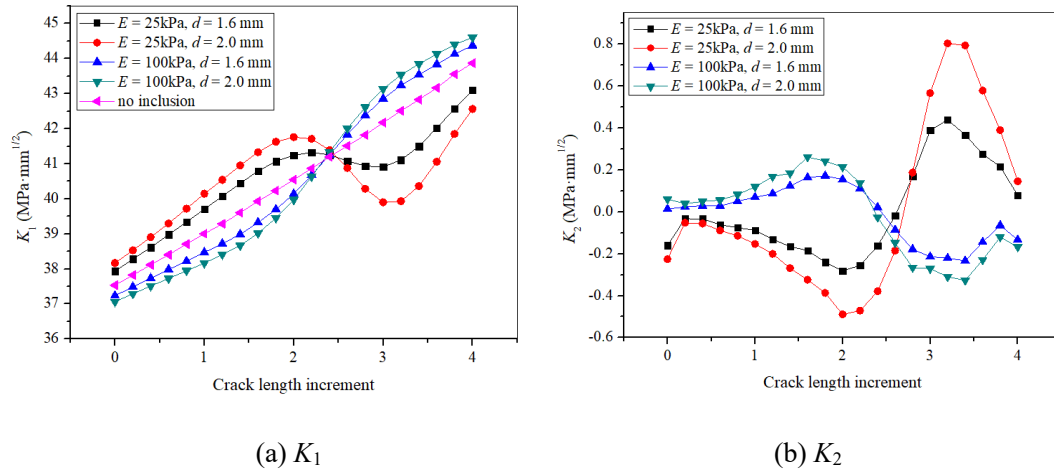


Fig. 10 The variation of SIFs at the macrocrack tip during the crack growth process in presence of a microinclusion.

Conclusions

In this paper, a multi-level, adaptively refined mesh near the macrocrack tip where the microdefects exist is formulated by the combination of virtual node polygonal element shape function and quadtree meshes. The influence of the nearby microdefects on the macrocrack propagation have been numerically investigated by using VP-XFEM. The results show that, the location and geometric parameters of the nearby microdefects have great influence on the propagation of the macrocrack. Both of the amplification and shielding effect can be seen in different kinds of microdefects with different parameters.

References

- [1] Song SH, Bae JS. Fatigue crack initiation and propagation from hole defects. *Experimental Mechanics*, 1998, 38(3): 161-166.
- [2] Tsay LW, Shan YP, Chao YH, Shu WY. The influence of porosity on the fatigue crack growth behavior of Ti–6Al–4V laser welds. *Journal of Materials Science*, 2006, 41(22): 7498-7505.
- [3] Seo KJ, Choi BH, Lee JM, Shin SM. Investigation of the mixed-mode fatigue crack growth of a hot-rolled steel plate with a circular microdefect. *International Journal of Fatigue*, 2010, 32(7): 1190-1199.
- [4] Wu SC, Yu C, Yu PS, et al. Corner fatigue cracking behavior of hybrid laser AA7020 welds by synchrotron X-ray computed microtomography. *Materials Science and Engineering: A*, 2016, 651: 604-614.
- [5] Yang RS, Xu P, Yue ZW, et al. Dynamic fracture analysis of crack–defect interaction for mode I running crack using digital dynamic caustics method. *Engineering Fracture Mechanics*, 2016, 161: 63-75.
- [6] Rose LRF. Microcrack interaction with a main crack. *International Journal of Fracture*, 1986, 31(3): 233-242.

- [7] Gong SX. An exact formulation for the microcrack-finite main crack interaction. *International Journal of Fracture*, 1994, 66: R51-R56.
- [8] Meguid SA, Wang XD. On the dynamic interaction between a microdefect and a main crack. *Proc. R. Soc. Lond. A*, 1995, 448(1934): 449-464.
- [9] Tamuzs VP, Petrova VE. Modified model of macro–microcrack interaction. *Theoretical and applied fracture mechanics*, 1999, 32(2): 111-117.
- [10] Tamuzs VP, Petrova VE. On macrocrack–microdefect interaction. *International applied mechanics*, 2002, 38(10): 1157-1177.
- [11] Petrova V, Tamuzs V, Romalis N. A survey of macro-microcrack interaction problems. *Applied Mechanics Reviews*, 2000, 53(5): 117-146.
- [12] Liu G, Zhou D, Bao Y, et al. Multiscale analysis of interaction between macro crack and microdefects by using multiscale projection method. *Theoretical and Applied Fracture Mechanics*, 2017, 90: 65-74.
- [13] Meguid S A, Gaultier P E, Gong S X. A comparison between analytical and finite element analysis of main crack-microcrack interaction. *Engineering fracture mechanics*, 1991, 38(6): 451-465.
- [14] Biner S B. A FEM analysis of crack growth in microcracking brittle solids. *Engineering fracture mechanics*, 1995, 51(4): 555-573.
- [15] Soh A K, Yang C H. Numerical modeling of interactions between a macro-crack and a cluster of micro-defects. *Engineering fracture mechanics*, 2004, 71(2): 193-217.
- [16] Li X, Li X, Jiang X. Influence of a micro-crack on the finite macro-crack. *Engineering Fracture Mechanics*, 2017, 177: 95-103.
- [17] Portela A, Aliabadi M, Rooke D. The dual boundary element method: effective implementation for crack problem. *Int. J. Numer. Meth. Eng.*, 1991, 33: 1269-1287.
- [18] Belytschko T, Lu YY, Gu L. Crack propagation by element-free Galerkin methods. *Eng. Fract. Mech.*, 1995, 51: 295-315.
- [19] Moës N, Dolbow J, Belytschko T. A finite element method for crack growth without remeshing. *Int. J. Numer. Meth. Eng.*, 1999, 46: 131-150.
- [20] Teng Z H, Sun F, Wu S C, et al. An adaptively refined XFEM with virtual node polygonal elements for dynamic crack problems. *Computational Mechanics*, 2018(1–3):1-20.
- [21] Liu G, Zhou D, Guo J, et al. Numerical simulation of fatigue crack propagation interacting with micro-defects using multiscale XFEM. *International Journal of Fatigue*, 2018, 109:70-82.
- [22] Tang XH, Wu SC, Zheng C, Zhang JH. A novel virtual node method for polygonal elements. *Applied Mathematics and Mechanics-English Edition*, 2009, 30(10): 1233-1246.
- [23] Moës N, Dolbow J, Belytschko T. A finite element method for crack growth without remeshing. *Int J Numer Meth Eng*, 1999, 46: 131-150.

- [24] Sukumar N, Chopp DL, Moes N, Belytschko T. Modeling holes and inclusions by level sets in the extended finite element method. *Comput Methods Appl Mech Eng*, 2001, 190: 6183–200.
- [25] Moës N, Cloirec M, Cartraud P, et al. A computational approach to handle complex microstructure geometries. *Computer methods in applied mechanics and engineering*, 2003, 192(28-30): 3163-3177.
- [26] Jiang S, Du C, Gu C, Chen X. XFEM analysis of the effects of voids, inclusions and other cracks on the dynamic stress intensity factor of a major crack. *Fatigue & Fracture of Engineering Materials & Structure*, 2014, 37: 866-882.